

Raman-Enhanced Regenerative Ultrafast All-Optical Fiber XPM Wavelength Converter

Wei Wang, *Student Member*, Henrik N. Poulsen, Lavanya Rau, *Student Member*, Hsu-Feng Chou, John E. Bowers, *Fellow*, and Daniel J. Blumenthal, *Fellow, IEEE*

Abstract—The Raman gain enhancement of a regenerative ultrafast all-optical cross-phase modulation (XPM) wavelength converter (WC) is quantitatively investigated and experimentally demonstrated to operate error free at 40 and 80 Gb/s. The regenerative nature of the converter is shown by experimentally demonstrating a negative 2-dB power penalty at 80 Gb/s. It is also shown that the Raman gain greatly enhances the wavelength conversion efficiency at 80 Gb/s by 21 dB at a Raman pump power of 600 mW using 1 km of highly nonlinear fiber. An analytical theory based on nonlinear phase-shift enhancement of the fiber-effective length is presented and shows the relationship between a nonlinear enhancement and Raman gain as a function of pump power and fiber design parameters. Measured parameters are used in the analytical model, and a good fit between experiment and theory is shown for two different types of fiber: one dispersion-shifted and one highly nonlinear fiber. The ultrafast response time of Raman gain makes this technique applicable to fiber-based ultrafast WCs. In addition, the applicability to other nonlinear fiber wavelength conversion techniques is discussed.

Index Terms—Cross-phase modulation (XPM), nonlinear optics, optical fiber communication, Raman effect, wavelength conversion.

I. INTRODUCTION

ALL-OPTICAL wavelength conversion is a key function for ultra-high-capacity optical-time-division-multiplexing/ wavelength-division-multiplexing (OTDM/WDM) networks. The capability of predominantly leaving signals in the optical domain is one way of reducing power dissipation of transmission and switching systems that handle high-bit-rate data streams. In these networks, all-optical wavelength conversion will enable wavelength routing, wavelength reuse, and reduced contention [1], [2]. As the demand for higher capacity networks operating beyond 40 Gb/s increases, the requirements for wavelength converters (WCs) to operate at these higher bit rates with low chip, high extinction ratio, high signal-to-noise ratio (OSNR), and 2R (reamplification and reshaping) or 3R (reamplification, reshaping, and retiming) regeneration capability will become extremely important. There are mainly three kinds of media for all-optical wavelength conversion: semi-

conductor optical amplifier (SOA)-based converters [3]–[5], passive waveguide-based converters [6], and fiber-based converters. Among these three methods, fiber-based WCs have the most promising potential of attaining terabit-per-second performance due to the femtosecond response time of the fiber nonlinearity [7]. Previous ultra-high-speed wavelength conversion of return-to-zero (RZ) data has been demonstrated using four-wave mixing (FWM) in fiber [8], cross-phase modulation (XPM) in the nonlinear optical loop mirror (NOLM) [9], self-phase modulation (SPM) in fiber [10], and XPM in fiber [11]. Using FWM, it is not possible to convert an unknown wavelength to a predetermined wavelength. Using SPM, the wavelength conversion range is limited. The NOLM requires short pulses compared with the bit period and suffers from stability problems. Compared with these fiber-wavelength conversion methods, XPM-based WCs are more simple and robust.

It has been shown before that Raman assistance in highly nonlinear fiber promotes parametric amplification and wavelength conversion [12]. In this paper, it is demonstrated that XPM-based WCs can also benefit greatly from Raman gain. By combining Raman amplification with bulk-erbium-doped fiber amplifier (EDFA) amplification, the OSNR and extinction ratio of the conversion can be optimized. The enhancement of Raman gain on the XPM phase modulation is studied quantitatively, and measurements are shown to fit the theory very well. We first demonstrate 40-Gb/s wavelength conversion enhanced by Raman gain using 5 km of standard dispersion-shifted fiber (DSF). Then, using highly nonlinear DSF (HNLD SF), wavelength conversion at an 80-Gb/s data rate is demonstrated with an extended conversion bandwidth to almost the entire *C* band.

The paper is organized as follows. Section II describes the architecture of the Raman-gain-enhanced XPM WC. Its regenerative property is also discussed. Section III shows the analytical studies on the XPM enhancement from Raman gain based on effective-length analysis. Measurements are shown to fit the calculation for two types of fibers. Section IV shows error-free wavelength conversion experiment results at 40 and 80 Gb/s using these two fibers, and the conversion efficiency enhancement from Raman gain is measured in both cases. Finally, Section V concludes the paper, and the applicability of this technique to other nonlinear fiber conversion techniques is discussed.

II. RAMAN-ENHANCED XPM CONVERTER ARCHITECTURE

The basic idea of this WC is to use XPM in the DSF. Fig. 1 shows the architecture of the Raman-gain-enhanced wavelength

Manuscript received October 14, 2003; revised August 3, 2004. This work was supported in part by JDS Uniphase in partnership with the State of California under Micro Grant 01-005.

W. Wang, H. N. Poulsen, L. Rau, and D. J. Blumenthal are with the Optical Communications and Photonic Networks Group, Department of Electrical and Computer Engineering, University of California, Santa Barbara, CA 93106 USA (e-mail: wwang@engineering.ucsb.edu).

H.-F. Chou and J. E. Bowers are with the Ultra Fast Optoelectronics Group, Department of Electrical and Computer Engineering, University of California, Santa Barbara, CA 93106 USA.

Digital Object Identifier 10.1109/JLT.2005.843468

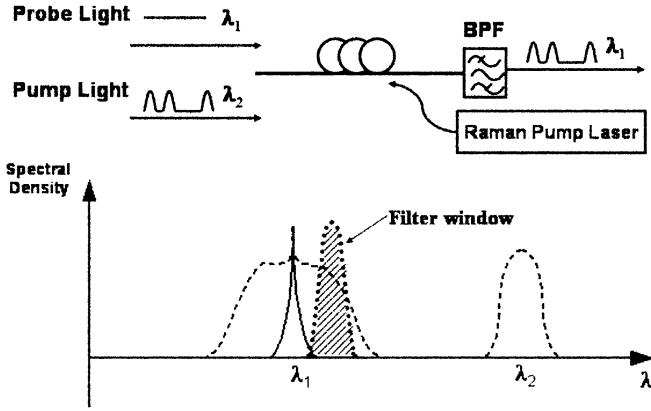


Fig. 1. XPM RE-WC architecture.

converter (RE-WC). It consists of one spool of nonlinear fiber, one Raman pump laser, and a bandpass filter (BPF). When the data pump light at wavelength λ_2 is combined with the continuous-wave (CW) probe light at λ_1 and sent through the fiber, XPM imposes sidebands onto the CW light. The Raman pump amplifies both the pump light and the probe light and significantly enhances the amount of XPM. The BPF is then used to select one of the sidebands and converts phase modulation into intensity modulation and, hence, transfers the signal data to the new wavelength. When very little power of the pulsed pump light is injected into the fiber, such as when there is a “zero” bit injected, the power transmitted through the filter window is minimized. However, when a “one” bit is injected, there will be enough XPM to broaden the spectrum of the CW so that the sideband overlaps the transmission window of the tunable filter and thus transmit light. This results in the nonlinear shape of the transfer function, which is, to some extent, determined by the transfer function of the filter used. Fig. 2 shows the sinusoidal-like nonlinear transfer function of this WC. The conversion process relies solely on the intensity change in the time domain, that is, an intensity change at one wavelength translated to a phase change at another wavelength. Any chirp in the input signal will not be transferred during the conversion, and the output pulse will therefore be very close to transform limited. The nonlinear transfer function will minimize the fluctuations in the top and bottom level of the signal due to the flatter characteristics of the transfer function at these power levels.

In the past, fiber-based wavelength converters have utilized bulk EDFA amplification prior to injecting the signal into the fiber in order to maximize the conversion efficiency. Due to the relatively low nonlinear coefficient of the fiber, high-power EDFAs are normally required. Besides the signal quality degradation from the amplifiers’ amplified spontaneous emission (ASE), their gain bandwidth is usually 30 nm and not flat. It is therefore complicated to obtain broad-band operation using these EDFAs. Compared with EDFAs, Raman amplifiers have been proved to have two merits: inherently low noise [13], [14] and flexible gain bandwidth (BW) [15], [16]. The idea of replacing or partially replacing the booster EDFA with Raman amplifiers for the WC comes from these merits. We can use the same spool of fiber as both Raman gain medium and XPM medium, and therefore Raman gain amplifies both pump and

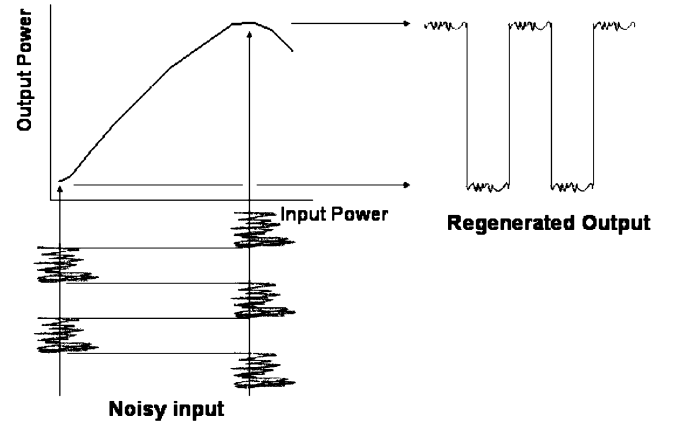


Fig. 2. Nonlinear transfer function of the WC.

probe signals at the same time the data is being imprinted to the new wavelength. Raman amplification exhibits lower signal-to-noise degradation to the WC in the sense that it can improve the signal-spontaneous beat noise at the receiver. Since Raman’s gain BW can be shaped by any combination of the selection of the pump wavelengths, the number of pumps utilized, and adjustment of the power levels of the pumps, we will be able to make a very broad-band WC. Other approaches to achieve this will have to involve waveband splitters and combiners and different types of amplifiers, which will be much more complicated.

III. THEORY OF OPERATION

A. Nonlinear Phase Change

To simplify the problem, we start from the fiber without the Raman pump. Considering the pulsed pump light and the CW probe light propagating in the fiber with the same polarization state, the nonlinear equations that govern their behaviors can be expressed as [7]

$$\frac{\partial A_s}{\partial z} + \frac{\alpha}{2} A_s + \frac{1}{v_{gs}} \frac{\partial A_s}{\partial t} = i\gamma(|A_s|^2 + 2|A_p|^2)A_s \quad (1)$$

$$\frac{\partial A_p}{\partial z} + \frac{\alpha}{2} A_p + \frac{1}{v_{gp}} \frac{\partial A_p}{\partial t} = i\gamma(|A_p|^2 + 2|A_s|^2)A_p \quad (2)$$

where A_s and A_p are the slowly varying complex field envelopes of the probe light and the pump light, α is the attenuation coefficient of the fiber, v_{gs} and v_{gp} are the group velocity of the two waves, and γ is the nonlinear coupling coefficient of the fiber. The two terms on the right-hand side of the equations are the results of nonlinear refractive index n_2 of the fiber with the first term corresponding to SPM and the second term corresponding to XPM. The general solution of (1) can be expressed as

$$A_s(z, t) = A_s(0, t - z/v_{gs}) \exp(-\alpha z/2) \exp(i\Delta\phi(z, t)). \quad (3)$$

If the pulse dispersion is neglected, the phase shift $\Delta\phi$ to the probe light at the end of fiber L induced by fiber nonlinearities is given by [7]

$$\Delta\phi = \gamma L_{\text{eff}}(P_s + 2P_p) \quad (4)$$

where L_{eff} is the effective length of the fiber, P_s is the probe power, and P_p is the pump power at the input of the fiber. The first term is caused by SPM, and the second term is by the effect of XPM. We call the second term $\Delta\phi_{\text{XPM}}$, which determines the conversion efficiency of this WC.

B. L_{eff} Enhancement, Simulation, and Measurements

When chromatic dispersion is neglected, $\Delta\phi_{\text{XPM}}$ is proportional to the nonlinear coefficient of the fiber, the effective length, and the pump wave power. Since γ is a fiber parameter, and the fixed input power is assumed, the only parameter enhanced by Raman gain is the effective length. L_{eff} is defined as [7]

$$L_{\text{eff}} = (1/P_p(0)) \int_0^L P_p(z) dz. \quad (5)$$

Without Raman pump, the expression of L_{eff} is

$$L_{\text{eff}}^{\text{noRA}} = (1 - e^{-\alpha L})/\alpha \quad (6)$$

which is fully determined by the loss of the fiber. When Raman pump coexists in the fiber, it extends L_{eff} by changing the power evolution of the signal $P_p(z)$ inside the fiber. As an example, Fig. 3 shows the simulated normalized power evolution of the signal inside the fiber with and without Raman gain. The simulation was performed for 1 km of fiber counterpumped with 300 mW of Raman pump power. The input signal was set at 1 mW for the simulation. From the definition, L_{eff} is the area under the curve. The shadow area between the two curves shows the amount of L_{eff} enhancement as a result of Raman gain.

If we only consider the WC pump light and the Raman pump light propagating inside the fiber, the coupling equations describing the energy transfer from the Raman pump to the WC pump can be written as

$$\frac{dP_p(z)}{dz} = -\alpha_p P_p(z) + \frac{g_R}{A_{\text{eff}}} P_p(z) P_{\text{Rp}}(z) \quad (7)$$

$$\frac{dP_{\text{Rp}}(z)}{dz} = \mp \left[\alpha_{\text{Rp}} P_{\text{Rp}}(z) + \frac{\omega_{\text{Rp}}}{\omega_p} \frac{g_R}{A_{\text{eff}}} P_p(z) P_{\text{Rp}}(z) \right] \quad (8)$$

where P_{Rp} is the Raman pump power, g_R is the Raman gain coefficient, and A_{eff} is the effective-mode area. The minus sign in (8) corresponds to copropagating pumping, i.e., the Raman pump propagating in the same direction as the signal. The plus sign corresponds to counterpumping. The last term in (8) corresponds to the pump depletion, which is the power the Raman pump transfers to the signal during the amplification process. Under the nonpump depletion assumption, namely when the input signal is small, this term can be ignored, and the coupled equations can be solved analytically. If the nonpump depletion assumption is not valid, there is no analytical solution, and numerical methods have to be used. Assuming that the Raman pump power is P , the effective length with Raman pumping can

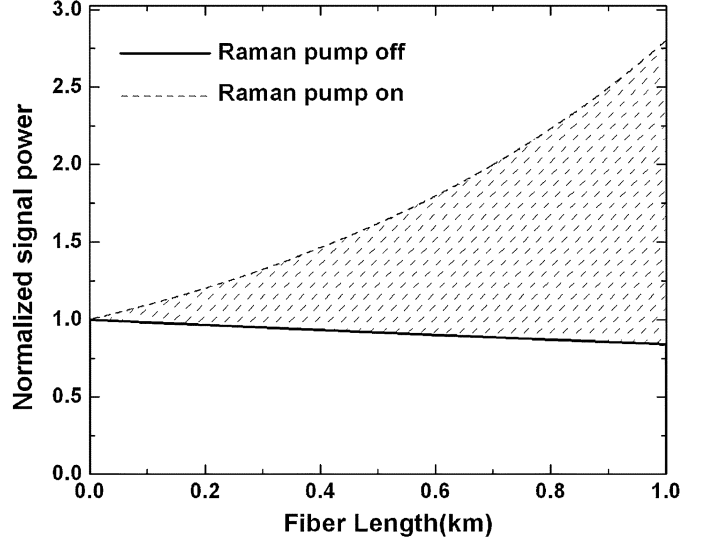


Fig. 3. Raman enhancement of the L_{eff} .

be calculated for both counterpumping and copumping cases as

$$L_{\text{eff}}^{\text{RAcounter}} = \int_0^L \exp \left[g_R \frac{P}{A_{\text{eff}}} \frac{e^{-\alpha_{\text{Rp}} L} (e^{\alpha_{\text{Rp}} z} - 1)}{\alpha_{\text{Rp}}} - \alpha_p z \right] dz \quad (9)$$

$$L_{\text{eff}}^{\text{RAco}} = \int_0^L \exp \left[g_R \frac{P}{A_{\text{eff}}} \frac{(1 - e^{\alpha_{\text{Rp}} z})}{\alpha_{\text{Rp}}} - \alpha_p z \right] dz. \quad (10)$$

We define the XPM enhancement factor E_{XPM} as the ratio between $\Delta\phi_{\text{XPM}}$ with and without Raman gain. From the analyses presented, E_{XPM} is also the ratio between L_{eff} with and without Raman gain. We calculated E_{XPM} as a function of Raman pump power for two types of fibers under both pumping conditions. The results are shown in Fig. 4. The fiber parameters used for the calculation are shown in Table I.

The DSF we used in the experiments has a smaller effective-mode area than most standard DSF, which has a typical A_{eff} of around $50 \mu\text{m}^2$. As can be seen from Fig. 4, 5 km of DSF has a similar enhancement factor to only 1 km of highly nonlinear fiber (HNLf). In addition, the enhancement factor under a copumping condition is larger than that under a counterpumping condition for both fibers. The reason is that in the copumping case, the signal sees more pump power at the input of the fiber and the nonlinear interaction happens earlier and more efficiently. At very low Raman pump power levels, the difference between co-pumping and counterpumping cases is not very obvious. The difference becomes larger when the Raman pump power is increased as well as when the length of the fiber is extended.

For a fiber with unknown parameters, E_{XPM} can be measured. Since the information of E_{XPM} lies in the nonlinear phase broadening term and is closely related to the nonlinear coupling coefficient, any method that is capable of measuring the nonlinear coupling coefficient can also be used to measure E_{XPM} . To date, the nonlinear coefficient of the optical fibers has been measured by the SPM of a pulsed laser source [17], the SPM of

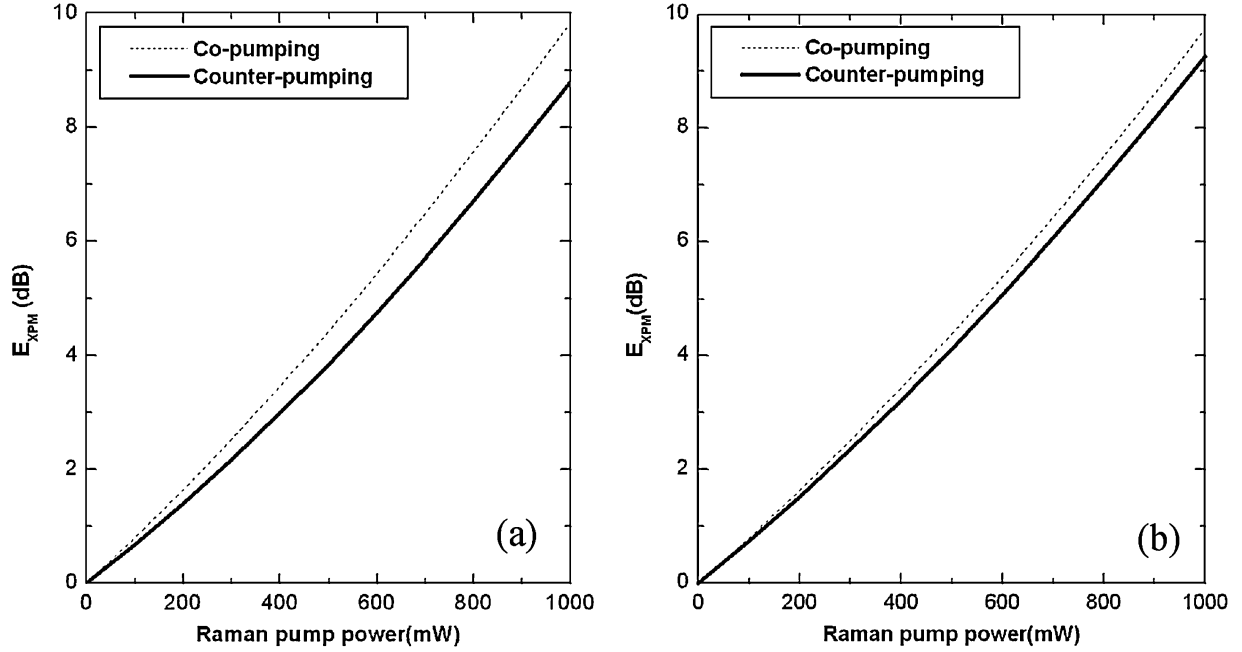


Fig. 4. Calculated XPM enhancement as a function of Raman pump power: (a) 5 km of DSF and (b) 1 km of HNLF.

TABLE I
SIMULATION PARAMETERS

Symbol	Standard DSF	HNLDSF
γ (1/km.W)	3.5	10.9
g_R ($\times 10^{-14}$ m/W)	2.088	5.03
L (km)	5	1
A_{eff} (μm^2)	23.5	11.8
α_{Rp} (dB/km)	0.4	0.95
α_p (dB/km)	0.25	0.75
D (1/ps.nm ² .km)	0.27	0.0167

dual CW light [18], the XPM method [19], the self-aligned interferometer (INT) method [20], and FWM [21]. We chose the method used by Boskovic *et al.* [18], which uses the SPM of the dual-frequency beat signals. Fig. 5 shows the typical measured spectrum at the output of the fiber.

The principle of this method can be described as follows. The fiber nonlinearity creates spectral sidebands, and the intensity ratio between the signal I_0 and the first sideband I_1 results in a nonlinear phase shift through

$$\frac{I_0}{I_1} = \frac{J_0^2(\Delta\phi) + J_1^2(\Delta\phi)}{J_1^2(\Delta\phi) + J_2^2(\Delta\phi)} \quad (11)$$

where $I_{0,1}$ are the peak intensity of the signal and the first sidebands, respectively, and J_n is the n th Bessel function. $\Delta\phi$ is the nonlinear phase shift and is given by

$$\Delta\phi = \frac{\omega_0}{c} \gamma L_{\text{eff}} P \quad (12)$$

where P is the power of the input dual-frequency beat signal. Since we can measure $\Delta\phi$ directly and extract L_{eff} for different Raman pump power levels, this method provides a direct way of measuring the XPM enhancement factor E_{XPM} for different

types of fibers. We use the similar setup as in [18] to measure $\Delta\phi$ as a function of input power P . Fig. 6 shows the measurement results for 1 km of HNLF for different Raman pump power levels. It shows a linear relation between $\Delta\phi$ and P , which fits well with (12), but only to some power level. Saturation happens when the assumption of nonpump depletion breaks down at high input powers, and the saturation power point depends on the Raman pump power. It can be seen that the slope of the linear region increases with Raman pump power and that the amount of this increase is the XPM enhancement factor. Fig. 7 shows the simulated and measured E_{XPM} for both types of fiber. To reduce the amount of relative intensity noise (RIN) transfer [22], we use the counterpumping scheme for the measurements. It is obvious that there is a good fit between the calculations and the measurements.

As discussed previously, Raman gain can be used to significantly enhance the XPM process and increase the conversion efficiency for this ultrafast WC. The amount of enhancement is strongly dependent on the fiber parameters, especially the effective-mode area, nonlinear coupling coefficient, fiber length, and the Raman gain coefficient. For 1 km of HNLF, the increase of XPM is as large as 6 dB for 600 mW of Raman pump power.

IV. EXPERIMENTAL DEMONSTRATION

To demonstrate the effect of Raman enhancement on the fiber XPM WC, we now perform Raman-enhanced wavelength conversion using two types of fibers described in the previous section at 40 and 80 Gb/s. Due to the higher Raman gain coefficient and smaller effective-mode area of the HNLF, a similar amount of Raman enhancement factor can be achieved using 1 km of HNLF instead of 5 km of standard DSF. Furthermore, due to the shorter length required and higher nonlinear coefficient of the HNLF, we were able to convert to a much broader BW at a higher bit rate using the HNLF.

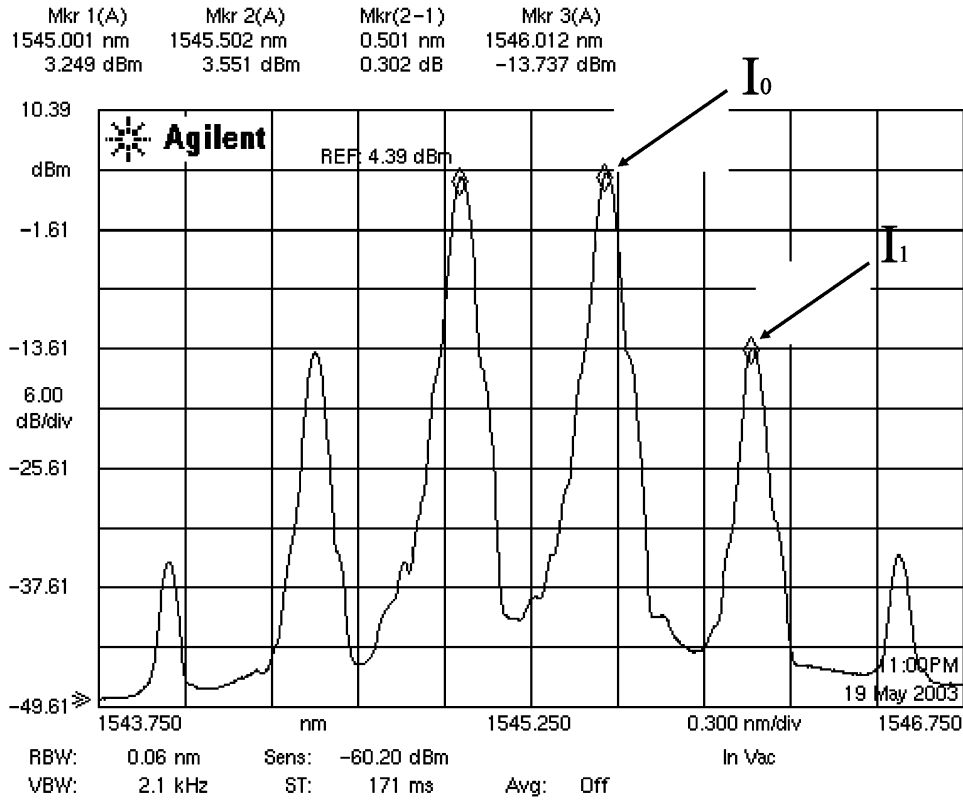


Fig. 5. Typical measured transmitted spectrum for the nonlinear wave mixing in DSF.

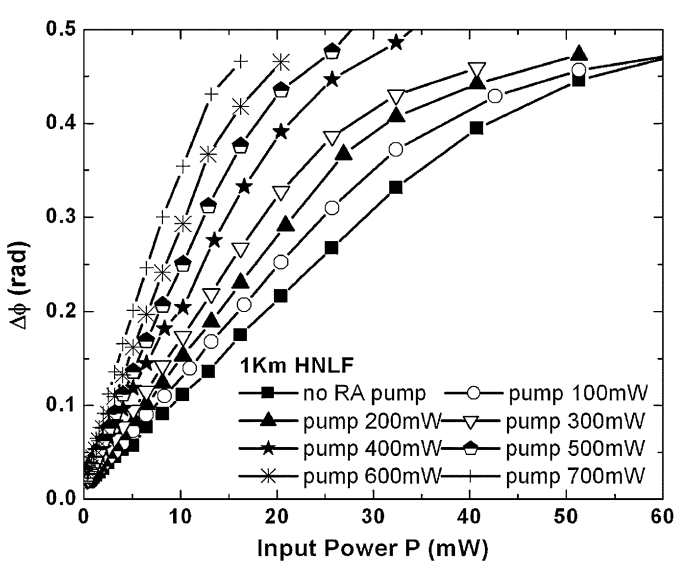


Fig. 6. Measured phase shift of different Raman pump levels for counterpumped 1 km of HNLF.

A. 40-Gb/s RE-WC Using 5 km of Standard DSF

The first WC experiment is demonstrated at 40 Gb/s with 5 km of standard DSF, and the experimental setup is shown in Fig. 8. An actively mode-locked fiber-ring laser was used to generate pulses with 8-ps pulsewidth at a 10-GHz repetition rate at 1554 nm. A subsequent modulator was used to encode 10-Gb/s pseudorandom bit sequence (PRBS) $2^{31} - 1$ data, and a passive 10–40-Gb/s split delay and time interleave multiplexer was used

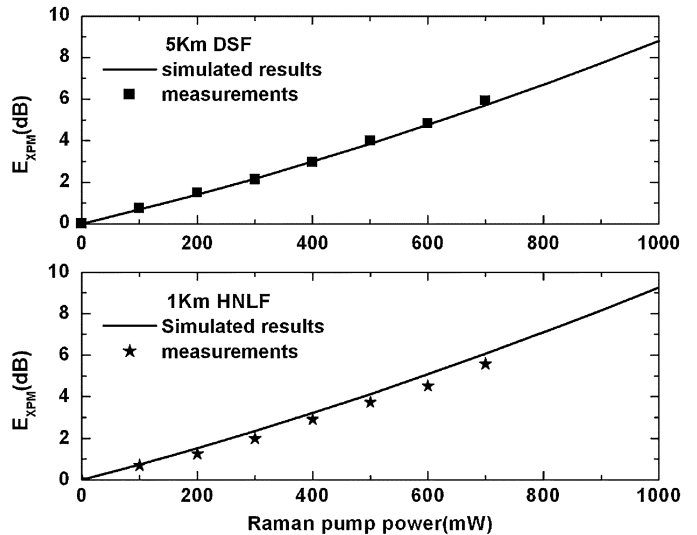


Fig. 7. Compare calculation and measurement results of XPM enhancement for both DSF and HNLF.

to generate a 40-Gb/s data stream. The 40-Gb/s data was combined with CW light from a tunable external-cavity laser and injected into the fiber Raman amplifier. The amplifier consists of an isolator, 5 km of DSF with a zero-dispersion wavelength of 1560 nm, a Raman pump laser with a maximum output power of 850 mW and a RIN of -110 dB/Hz. The Raman pump was set at 670 mW for the bit-error-rate (BER) measurements. As discussed previously, a counterpropagating pump scheme was used to minimize the effect of pump fluctuation on the amplifier gain. The wavelength of the converted signal was chosen

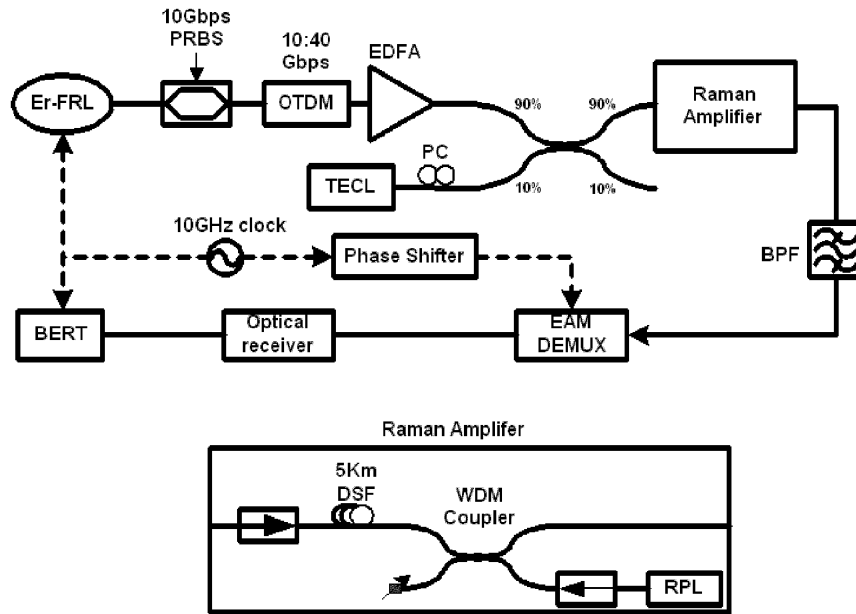


Fig. 8. Experimental setup for 40-Gb/s wavelength conversion.

to be close to the gain maximum on the gain curve. Two isolators, one in front of the fiber and the other after the WDM coupler, were positioned to reduce the amount of double-Raleigh backscattering (DRBS) noise at higher pump power levels. A 0.4-nm BPF was used to select one of the sidebands, and a sampling oscilloscope was used to measure the pulse characteristics. An electroabsorption modulator (EAM) with a 15-ps switching window was used to demultiplex the 40-Gb/s signal into four 10-Gb/s signal streams for BER measurements. Fig. 9 shows the measured BER of the four demultiplexed channels for wavelength conversion from 1554 to 1558 nm and the eye patterns of the original and the wavelength-converted 40-Gb/s signal. The output eye diagram shows the regenerative quality of the converter through a reduction in the output eye amplitude variation. The measured power penalty of the converted 40-Gb/s data relative to the original data is less than 1 dB.

To estimate the influence of Raman gain on the converter performance, the electrical signal-to-noise ratio (ESNR) was measured with respect to the Raman pump power. Fig. 10 shows the ESNR versus input peak power at three different Raman gain levels together with the nonlinear transfer function of the WC. The ESNR was measured by taking the ratio of the average power in the fundamental 10-GHz tone to the average power in the noise BW from 50 MHz to 9.9 GHz. It can be seen that conversion efficiency increases with higher Raman gain when the WC is appropriately pumped such that SPM is managed. The output ESNR can be maintained over a wide range of input signal by varying the Raman pump power.

Further measurements were performed to characterize the enhancement of Raman gain on the conversion efficiency of this WC. Fig. 11 shows the spectrum at the output of the fiber with Raman pump power of 0, 300, and 600 mW, respectively (resolution BW: 0.1 nm). The 40-GHz frequency tones are very clear on both sides of the CW probe due to XPM, and a significant XPM sideband increase can be observed when the Raman pump power is increased. We measured the conversion efficiency enhancement as a function of Raman pump power by comparing

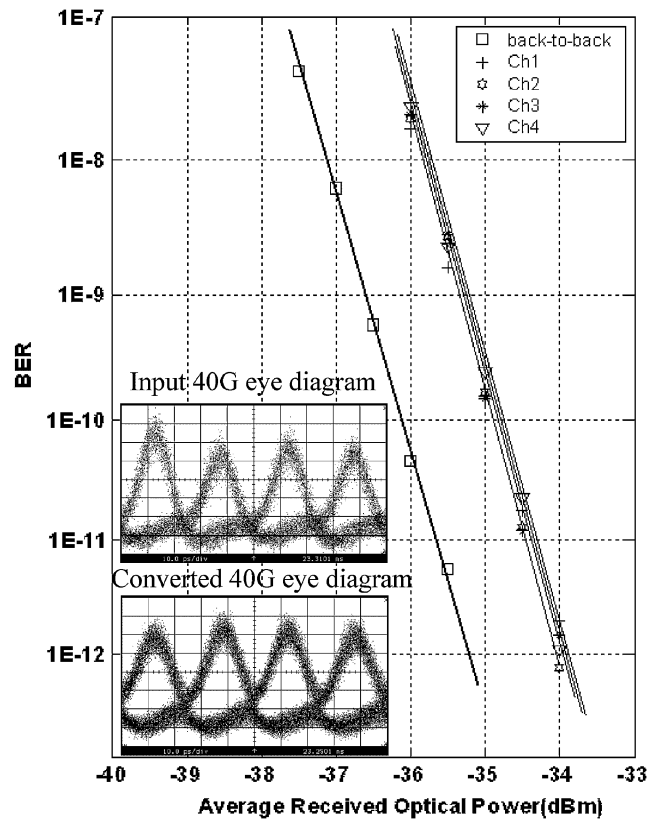


Fig. 9. BER measurements and eye diagrams for wavelength conversion of 40-Gb/s data from 1554 to 1558 nm.

the sideband power level on the spectrum analyzer at different Raman pump power levels with the one without Raman gain. Fig. 12 shows the small-signal Raman gain at 1558 nm and the conversion efficiency enhancement as a function of Raman pump power for the 40-Gb/s experiment. Since the Raman gain has a broad gain BW, both the pump light and the probe light are amplified, and the total conversion efficiency enhancement is higher than the E_{XPM} we defined in Section III. For example,

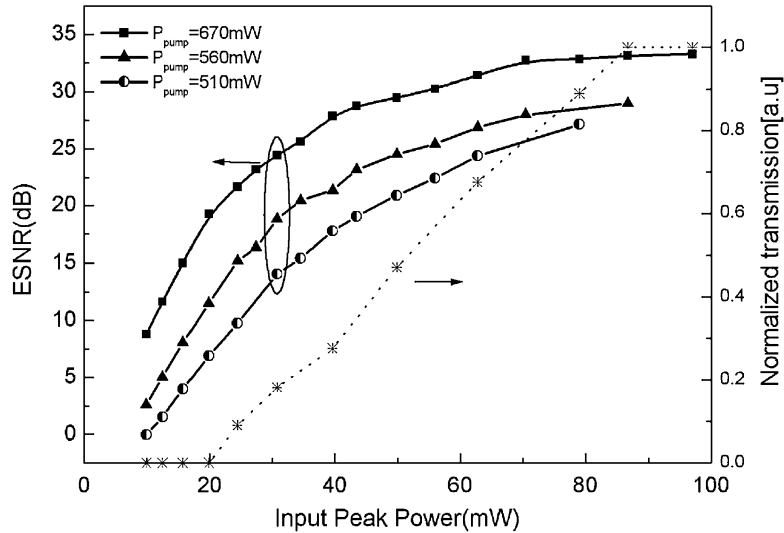


Fig. 10. ESNR and transmission versus input peak power for three different Raman pump power.

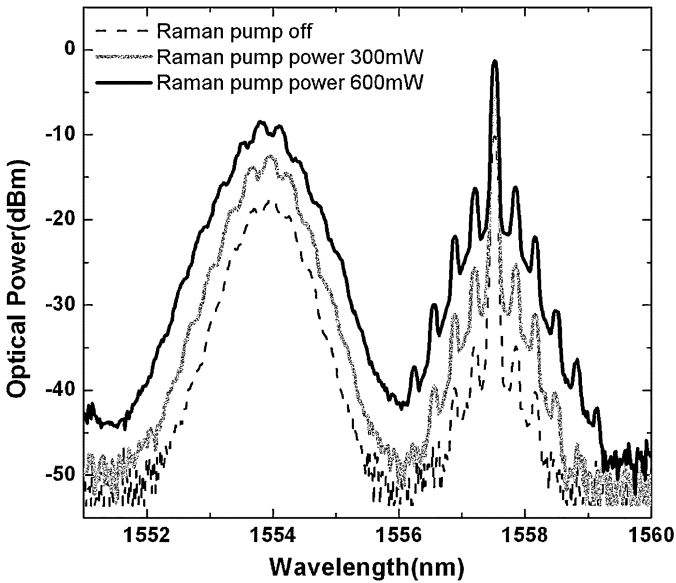


Fig. 11. Spectrum at the output of the RE-WC with different Raman pump power (resolution BW: 0.1 nm).

at a Raman pump power of 600 mW, the small-signal Raman gain is around 10 dB, the E_{XPM} is 5 dB for 5 km of DSF, but the conversion efficiency enhancement is 18 dB.

B. 80-Gb/s RE-WC Using 1 km of HNLF

If pulse dispersion and loss is ignored, the frequency shift of the CW probe light for Gaussian pump pulses can be related as [23]

$$\Delta f \propto P_{in}L[\exp(-(t - \beta)^2) - \exp(-t^2)]/\beta \quad (13)$$

where P_{in} is the input power and L the fiber length. The walk-off time β and the time t are normalized to the $1/e$ half-width of the input pulse. In this equation, the increase of β will decrease the conversion efficiency, so a shorter fiber is preferred for this WC in order to minimize the walk-off effect and improve the stability. As discussed previously, the HNLF can generate the same amount of nonlinear phase change and Raman enhancement

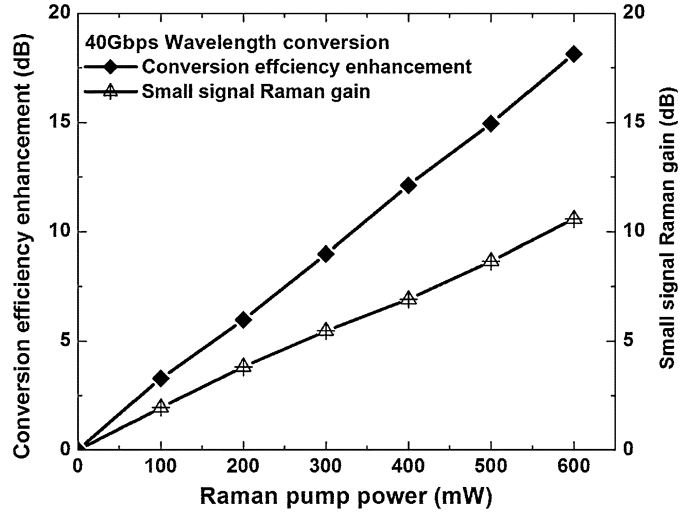


Fig. 12. Conversion enhancement and small-signal Raman gain versus Raman pump power for 40-Gb/s RE-WC.

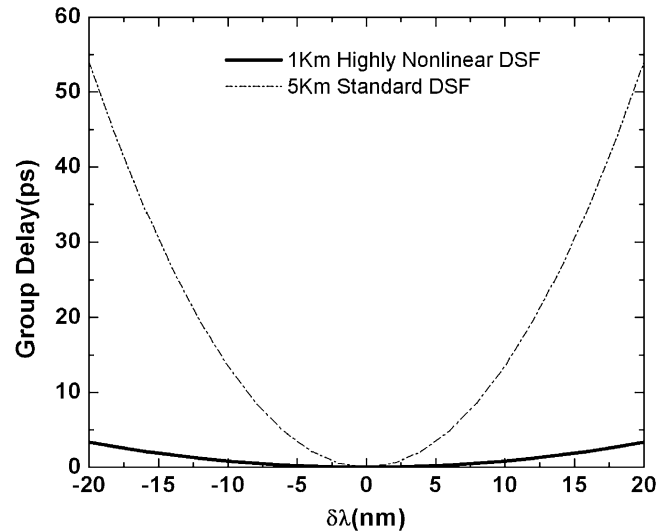


Fig. 13. Walk-off time versus wavelength difference for 5-km DSF and 1-km HNLF.

factor as a much longer standard DSF. Fig. 13 shows the calculated walk-off time of 5 km DSF and 1-km HNLF, assuming

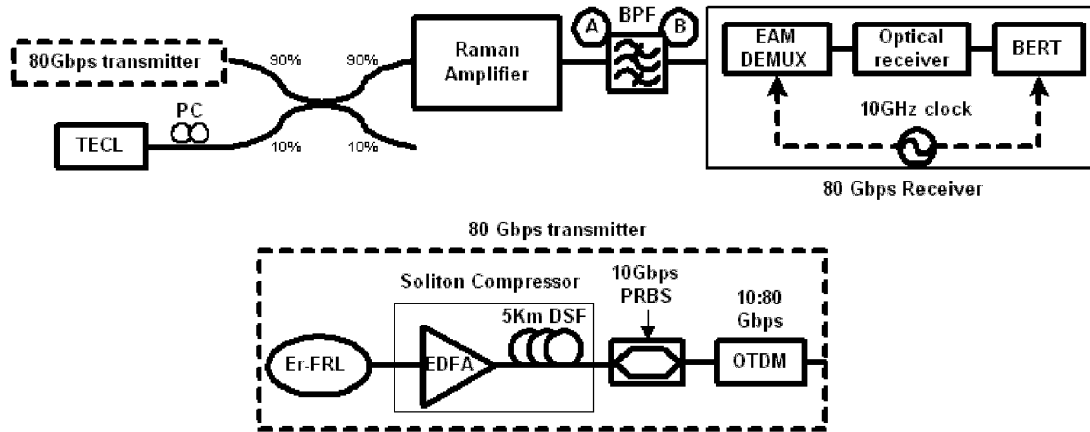


Fig. 14. Experimental setup for 80-Gb/s wavelength conversion.

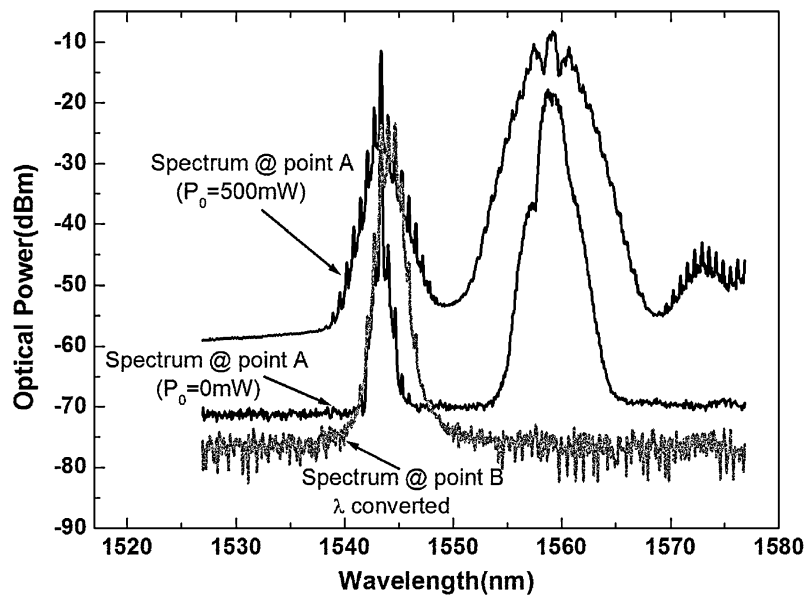


Fig. 15. Spectrum at point A (with Raman pump ON/OFF) and B of the WC in Fig. 14.

they have the same zero-dispersion wavelength. It is seen that the WC shows a substantial improvement when a shorter HNLFF is used instead of the normal DSF. For the HNLFF, the required power and the converted pulse width change are smaller over a broader wavelength range of interest due to a much lower walk-off. In addition, the decreased length of the HNLFF helps increase the mechanical stability of the WC.

Utilizing only 1 km of HNLFF, we demonstrate wavelength conversion over almost the entire C band at 80 Gb/s. The experimental setup is similar to the setup for 40-Gb/s WC, which is shown in Fig. 14. The mode-locked fiber-ring laser generates high-quality transform-limited pulses around 5 ps, which are not suitable for 80-Gb/s signal generation and were therefore compressed to 2 ps using soliton compression. The soliton compressor consists of an EDFA and 5 km of DSF. The HNLFF has a zero-dispersion wavelength at 1550 nm. The BPF we used in this experiment has a 3-dB BW of 1.2 nm. The optical spectrum measured after the HNLFF with and without Raman gain is shown in Fig. 15. A significant XPM sideband increase was observed with 500-mW Raman pump power. At a pump power of 350 mW, the calculated small-signal Raman

gain was around 6 dB, and E_{XPM} was measured to be around 3 dB, whereas the measured conversion efficiency enhancement was 10 dB. It clearly demonstrates the ability of the Raman gain to enhance the XPM wavelength conversion process without imposing any bit rate limit to the converter at the bit rates used in this paper.

Demultiplexing the 80-Gb/s signal into eight 10-Gb/s signals for BER measurements was achieved by using an EAM with a 7.5-ps-wide switching window. Fig. 16(a) shows the BER for the wavelength conversion from 1559 to 1545 nm. A negative 2-dB power penalty at $\text{BER} = 10^{-9}$ was measured for all eight channels compared to back-to-back measurements of the 80-Gb/s soliton-compressed signals. Fig. 16(b) shows the eye patterns of the original and the wavelength-converted 80-Gb/s signals. There is no visible difference between them. Fig. 16(c) shows the eye diagrams of the eight demultiplexed 10-Gb/s channels, which are all clear, open, and similar to each other. Eye patterns were measured with a 50-GHz digital sampling scope and a 40-GHz photodetector. The tuning characteristic of this WC was measured by varying the CW light from 1535 to 1555 nm in 2-nm steps. The converted pulsewidths were

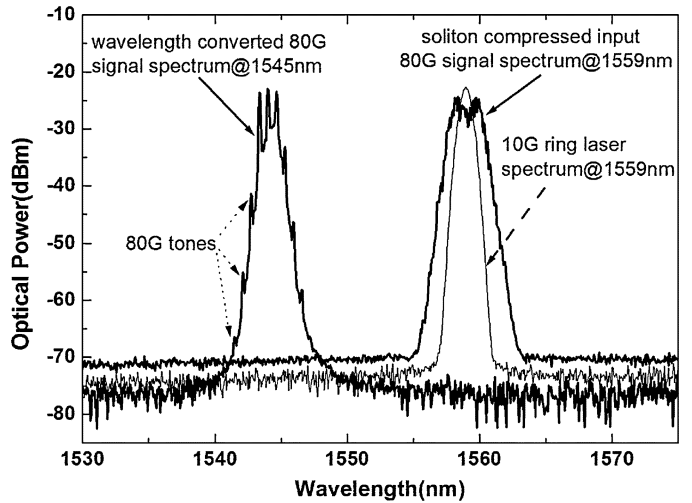
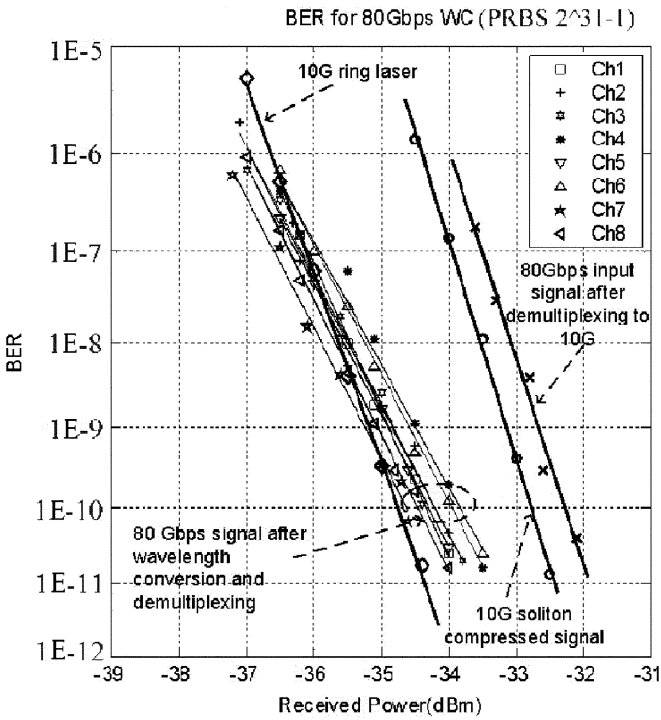


Fig. 17. Optical spectrum of the original and the wavelength-converted signal (resolution BW: 0.1 nm).

The negative power penalty exhibited by the WC can be explained by the nonlinear transfer function of the WC. However, the reshaping capability is not only observed in the time domain but also in the spectral domain. This behavior is clearly seen from Fig. 17, showing the optical spectrum of the original and the wavelength-converted signal at 80 Gb/s. The spectrum after soliton compression was significantly broadened, displaying a large amount of chirp. As a result, the receiver sensitivity was degraded by 2 dB to -33.2 dBm at $BER = 1E - 9$, compared with the original 10-GHz ring laser sensitivity of -35.2 dBm. After passively multiplexing the compressed pulse to 80 Gb/s, the input signal at 1559 nm was directly demultiplexed to 10 Gb/s, and the BER was measured for one of the eight demultiplexed channels. It showed a receiver sensitivity of -32.7 dBm. The 0.5-dB power penalty compared with the 10-Gb/s compressed pulse is mainly brought by the multiplexing and the demultiplexing processes. The regenerative capability of the WC is shown by the BER curves of the demultiplexed wavelength-converted signal, lying close to the original ring laser BER curve position, with an averaged receiver sensitivity of -34.9 dBm.

Similar measurements were performed to characterize the Raman enhancement on the conversion efficiency for the 1 km of HNLFF at 80 Gb/s as we did for the standard DSF. Fig. 18 shows the small signal Raman gain at 1545 nm and the conversion efficiency enhancement as a function of Raman pump power for this experiment. At a Raman pump power of 600 mW, a total conversion efficiency enhancement of 21 dB was achieved.

V. DISCUSSION AND CONCLUSION

Raman enhancement for a regenerative WC based on the nonlinear effects in fiber has been quantitatively studied and experimentally demonstrated. The first experiment was performed using standard DSF. DSFs are designed for transmission rather than for nonlinear signal processing and have two drawbacks for this kind of applications: 1) they have relatively low nonlinear coefficient and 2) they have fairly large dispersion slope. As a

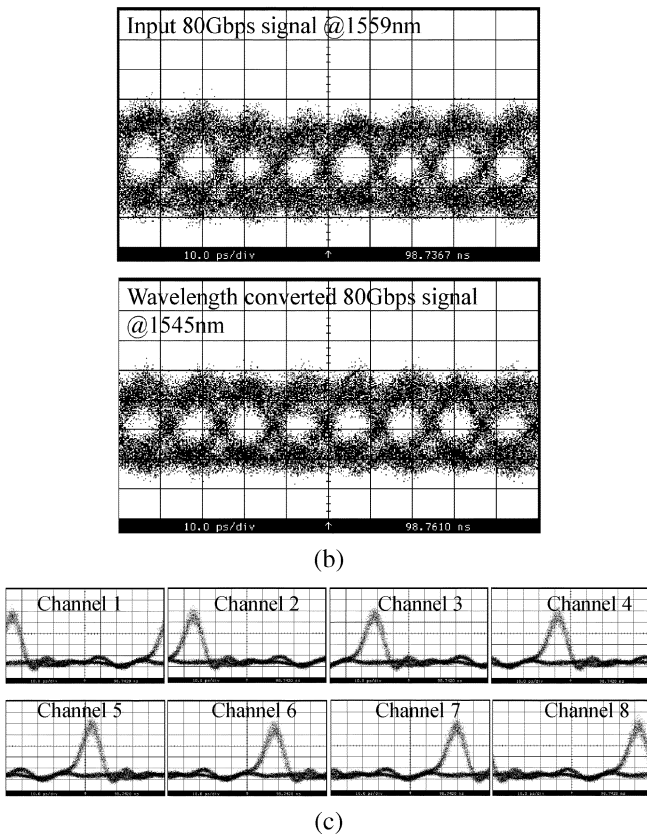


Fig. 16. (a) BER measurements for wavelength conversion of 80-Gb/s data from 1559 to 1545 nm. (b) Eye diagrams of input and wavelength-converted signal at 80-Gb/s (time: 10 ps/div). (c) Eye diagrams of converted 80-Gb/s signal demultiplexed to eight 10-Gb/s channels (10 ps/div).

measured to be 3.75 ps with less than 25% variation over the output wavelength range. The converted pulses were slightly broadened due to the converter output filter BW but maintained values less than 6 ps minimizing the intersymbol interference at 80 Gb/s.

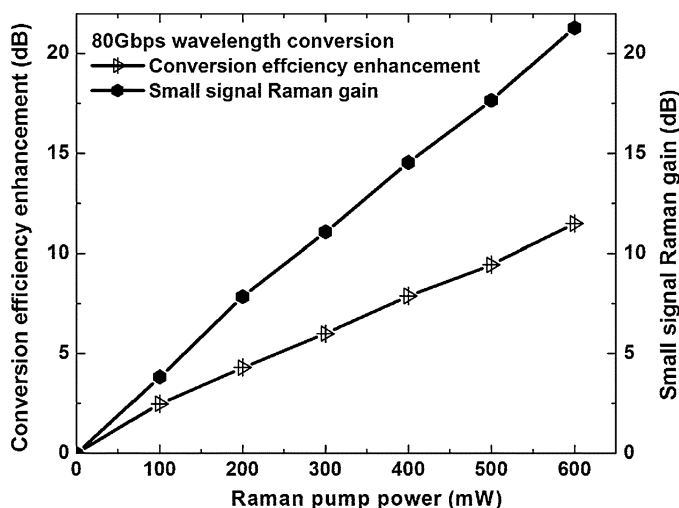


Fig. 18. Conversion enhancement and small-signal Raman gain versus Raman pump power for 80-Gb/s RE-WC.

result of the low nonlinear coefficient, the length of the fiber required for certain conversion efficiency is large for a given pump power. Combined with large-dispersion slope, this makes appreciable conversion BW achievable small. On the other hand, the HNLFF is designed to enhance the nonlinear effects in fibers. Higher nonlinearity reduces the power or fiber length required to achieve the same efficiency. Besides this, the dispersion is also reduced, resulting in wider conversion BW. Regenerative wavelength conversion at an 80-Gb/s rate over almost the entire *C* band was demonstrated using 1 km of HNLFF. Raman gain was shown to be able to significantly enhance the XPM process without posing any bit rate limitation to the WC. Due to the simple design and flexible assignment of wavelength bands for Raman amplifiers, Raman enhancement can be another powerful method next to holey fibers (HFs) for all kinds of nonlinear optical devices based on third-order nonlinear effects in fiber for fiber-optic communication systems. Recent developments in the design and fabrication of HF have provided a fiber with much higher nonlinearity per unit length than HNLFFs. Using fibers with such high nonlinearity would further decrease the length required to enable wavelength conversion or enable operation at much lower power levels. Due to the high Raman gain coefficient and small effective-mode area for HFs, the Raman gain per unit length is much higher. Future development of fiber with high nonlinear coefficient, small effective-mode area, large Raman gain coefficient, and low-dispersion slope will further decrease the power length product requirement for the WC and extend the conversion BW. We will be able to make a compact all-Raman-pumped WC that will be very versatile and efficient.

ACKNOWLEDGMENT

The authors would like to thank L. Gruner-Nielsen from OFS for the highly nonlinear fiber.

REFERENCES

- [1] A. Jourdan, F. Masetti, M. Garnot, G. Soulage, and M. Sotom, "Design and implementation of a fully reconfigurable all-optical crossconnect for high capacity multi-wavelength transport networks," *J. Lightw. Technol.*, vol. 14, no. 6, pp. 1198–1206, Jun. 1996.
- [2] P. E. Green, L. A. Coldren, C. M. Johnson, J. G. Lewis, C. M. Miller, J. F. Morrison, R. Olshansky, R. Ramaswami, and E. H. Smith, "All-optical packet-switched metropolitan-area network proposal," *J. Lightw. Technol.*, vol. 11, pp. 754–763, May 1993.
- [3] M. L. Masanovic, V. Lal, J. S. Barton, E. J. Skogen, L. A. Coldren, and D. J. Blumenthal, "Monolithically integrated Mach-Zender interferometer wavelength converter and widely tunable laser in InP," *IEEE Photon. Technol. Lett.*, vol. 15, no. 8, pp. 1117–1119, Aug. 2003.
- [4] J. Leuthold, C. H. Joyner, B. Mikkelsen, G. Raybon, J. L. Pleumeekers, B. I. Miller, K. Dreyer, and C. A. Burrus, "100 Gbit/s all-optical wavelength conversion with integrated SOA delayed-interference configuration," *Electron. Lett.*, vol. 36, pp. 1129–1130, 2000.
- [5] J. M. Tang and K. A. Shore, "A simple scheme for polarization insensitive four-wave mixing in semiconductor optical amplifiers," *IEEE Photon. Technol. Lett.*, vol. 11, no. 9, pp. 1123–1125, Sep. 1999.
- [6] J. Yamawaku, H. Takara, T. Ohara, K. Sato, A. Takada, T. Morioka, O. Tadanaga, H. Miyazawa, and M. Asobe, "Simultaneous 25 GHz-spaced DWDM wavelength conversion of 1.03 Tbit/s (103 × 10 Gbit/s) signals in PPLN waveguide," *Electron. Lett.*, vol. 39, no. 24, pp. 1144–1145, 2003.
- [7] G. P. Agrawal, *Nonlinear Fiber Optics*, 2nd ed. San Diego, CA: Academic, 1995.
- [8] O. Aso and S. Namiki, "Recent advances of ultra-broadband fiber-optics wavelength converters," presented at the Eur. Conf. Optical Communication (ECOC), Munich, Germany, Sep. 3–7, 2000. Paper ThA3.
- [9] J. Yu, X. Zheng, C. Peucheret, A. Clausen, H. Poulsen, and P. Jeppesen, "All-optical wavelength conversion of short pulses and NRZ signals based on a nonlinear optical loop mirror," *J. Lightw. Technol.*, vol. 18, no. 7, pp. 1007–1017, Jul. 2000.
- [10] P. V. Mamyshev, "All-optical data regeneration based on self-phase modulation effect," in *Proc. Eur. Conf. Optical Communication (ECOC)*, 1998, pp. 475–476.
- [11] B. E. Olsson, P. Ohlen, L. Rau, and D. J. Blumenthal, "A simple and robust 40-Gb/s wavelength converter using fiber cross-phase modulation and optical filtering," *IEEE Photon. Technol. Lett.*, vol. 12, no. 7, pp. 846–848, Jul. 2000.
- [12] D. A. Chestnut, C. R. S. Matos, and J. R. Taylor, "Raman-assisted fiber optical parametric amplifier and wavelength converter in highly nonlinear fiber," *J. Opt. Soc. Amer. B, Opt. Phys.*, vol. 19, no. 1901, 2002.
- [13] H. Masuda, S. Kawai, and K.-I. Suzuki, "Optical SNR enhanced amplification in long-distance recirculating-loop WDM transmission experiment using 1580 nm band hybrid amplifier," *Electron. Lett.*, vol. 35, pp. 411–412, 1999.
- [14] M. Nissov, C. R. Davidson, K. Rottwitz, R. Menges, P. C. Corbett, D. Innis, and N. S. Bergano, "100 Gb/s (10 × 10 Gb/s) WDM transmission over 7200 km using distributed Raman amplification," in *Proc. Eur. Conf. Optical Communication (ECOC)*, vol. 5, 1997, pp. 9–12.
- [15] C. R. S. Fludger, V. Handerek, and R. J. Mears, "Ultra-wide bandwidth Raman amplifiers," in *Optical Fiber Communication (OFC) Conf. Tech. Dig.*, 2002, pp. 60–62. Paper TuJ3.
- [16] T. Naito, T. Tanaka, K. Torii, N. Shimojoh, H. Nakamoto, and M. Suyama, "A broadband distributed raman amplifier for bandwidths beyond 100 nm," in *Optical Fiber Communication (OFC) Conf. Tech. Dig.*, 2002, pp. 116–117. Paper TuR1.
- [17] K. S. Kim, R. H. Stolen, W. A. Reed, and K. W. Quoi, "Measurement of the nonlinear index of silica-core and dispersion-shifted fibers," *Opt. Lett.*, vol. 19, pp. 257–259, 1994.
- [18] A. Boskovic, S. V. Chernikov, and J. R. Taylor, "Direct continuous-wave measurement of n_2 in various types of telecommunication fiber at 1.55 micron," *Opt. Lett.*, vol. 21, no. 24, pp. 1966–1968, 1996.
- [19] T. Kato, Y. Suetsugu, M. Takagi, E. Sasaoka, and M. Nishimura, "Measurement of the nonlinear refractive index in optical fiber by the cross-phase-modulation method with depolarized pump light," *Opt. Lett.*, vol. 20, pp. 988–991, 1995.
- [20] C. Vinegoni, M. Wegmuller, and N. Gisin, "Measurement of the nonlinear coefficient of standard SMF, DSF, and DCF fiber using a self-aligned interferometer and a Faraday mirror," *IEEE Photon. Technol. Lett.*, vol. 13, no. 12, pp. 1337–1339, Dec. 2001.
- [21] L. Prigent and J. Hamaide, "Measurement of fiber nonlinear Kerr coefficient by four-wave mixing," *IEEE Photon. Technol. Lett.*, vol. 5, no. 9, pp. 1092–1095, Sep. 1993.

- [22] C. R. S. Fludger, V. Handerek, and R. J. Mears, "Pump to signal RIN transfer in Raman fiber amplifiers," *J. Lightw. Technol.*, vol. 19, no. 8, pp. 1140–1148, Aug. 2001.
- [23] P. Ohlen, B. E. Olsson, and D. J. Blumenthal, "Wavelength dependence and power requirements of a wavelength converter based on XPM in a dispersion-shifted optical fiber," *IEEE Photon. Technol. Lett.*, vol. 12, no. 5, pp. 522–524, May 2000.

Lavanya Rau (S'03), photograph and biography not available at the time of publication.

Hsu-Feng Chou, photograph and biography not available at the time of publication.

Wei Wang (S'01), photograph and biography not available at the time of publication.

John E. Bowers (F'93), photograph and biography not available at the time of publication.

Henrik N. Poulsen, photograph and biography not available at the time of publication.

Daniel J. Blumenthal (M'97–F'03), photograph and biography not available at the time of publication.